chemosensors

Article

SO_2 Detection over a Wide Range of Concentrations: An Exploration on MOX-Based Gas Sensors

Arianna Rossi [1,*], Elena Spagnoli [1], Alan Visonà [1], Danial Ahmed [1], Marco Marzocchi [2], Vincenzo Guidi [1] and Barbara Fabbri [1,*]

[1] Department of Physics and Earth Sciences, University of Ferrara, Via Saragat 1/C, 44122 Ferrara, Italy; elena.spagnoli@unife.it (E.S.); alan.visona@edu.unife.it (A.V.); danial.ahmed@unife.it (D.A.); vincenzo.guidi@unife.it (V.G.)
[2] Sacmi Imola S.C., Olfactory Systems, Via Selice Provinciale, 17/a, 40026 Imola, Italy; marco.marzocchi@sacmigroup.com
* Correspondence: arianna.rossi@unife.it (A.R.); barbara.fabbri@unife.it (B.F.)

Abstract: Noxious gases such as sulfur-containing compounds can inflict several different adverse effects on human health even when present at extremely low concentrations. The accurate detection of these gases at sub-parts per million levels is imperative, particularly in fields where maintaining optimal air quality is crucial. In this study, we harnessed the capabilities of nanostructured metal-oxide semiconducting materials to detect sulfur dioxide, since they have been extensively explored starting from the last decades for their effectiveness in monitoring toxic gases. We systematically characterized the sensing performance of seven chemoresistive devices. As a result, the SnO_2:Au sensor demonstrated to be the most promising candidate for sulfur dioxide detection, owing to its highly sensitivity (0.5–10 ppm), humidity-independent behavior (30 RH% onwards), and selectivity vs. different gases at an operating temperature of 400 °C. This comprehensive investigation facilitates a detailed performance comparison to other devices explored for the SO_2 sensing, supporting advancements in gas detection technology for enhanced workplace and environmental safety.

Keywords: chemoresistive gas sensors; sulfur dioxide; metal oxides; air pollution; agriculture; fossil fuels plants

check for updates

Citation: Rossi, A.; Spagnoli, E.; Visonà, A.; Ahmed, D.; Marzocchi, M.; Guidi, V.; Fabbri, B. SO_2 Detection over a Wide Range of Concentrations: An Exploration on MOX-Based Gas Sensors. *Chemosensors* **2024**, *12*, 111. https://doi.org/10.3390/chemosensors12060111

Received: 10 May 2024
Revised: 7 June 2024
Accepted: 10 June 2024
Published: 14 June 2024

Copyright: © 2024 by the authors. Licensee MDPI, Basel, Switzerland. This article is an open access article distributed under the terms and conditions of the Creative Commons Attribution (CC BY) license (https://creativecommons.org/licenses/by/4.0/).

1. Introduction

Sulfur oxides (SO_x) are one of the major contributors to atmospheric pollution, including acid rain and smog formation [1]. Indeed, the oxidation of SO_2 leads to the formation of sulfuric acid and fine particulate matter (PM2.5, particulate matter less than or equal to 2.5 μm in diameter). This can have ecological impacts on soil, forests, and freshwater. Moreover, this category of pollutants is strongly harmful to human beings because inhaled SO_2 can easily be hydrated in the respiratory tract, producing sulfurous acid that subsequently dissociates to form its derivatives, bisulfite and sulfite anions [2], which can cause damage and increase chronic obstructive pulmonary diseases, e.g., pneumonia and acute bronchitis, and daily mortality [3]. The impact on human health motivated the low Threshold Limit Values, i.e., the Short-Term Exposure Limit (TLV-STEL) and the Permission Exposure Limit Time-Weighted Average (PEL-TWA) for SO_2 are 0.25 parts per million (ppm) and 5 ppm, respectively [4,5]. Therefore, many countries have established or are enacting stricter regulations to reduce the SO_2 emissions into the atmosphere [1].

In nature, the release of SO_x is caused by the combustion of carbonaceous fuels, which occurs in forest fires and volcanoes [6]. In the last case, SO_2 fluxes can be substantial in terms of atmospheric source strengths, for instance, the mean SO_2 flux from Mt. Etna in Sicily is equivalent to the total of anthropogenic SO_2 emissions from France, making it arguably the world's largest sustained point source emitter of SO_2. In addition to these inevitable natural contributions, there are also many anthropogenic sources of SO_x releases such as

the combustion of fossil fuels in power plants [7], for which the permissible concentration levels are 0.03 ppm (1 h) and 0.14 ppm (24 h) [8] in the case of electricity generation and industry boilers, respectively. Further contributions to SO_x emission came from oil refineries, domestic boilers, and motor vehicles, e.g., the European permissible limit of SO_2 produced from the automobiles exhaust ranges between 20 and 120 ppm/km [9]. Moreover, the extensive use of food additives leads to residual SO_2, generally in the range of 50–250 ppm [10], while the use of pesticides such as ammonium sulfate and potassium sulfate leads to the inevitable decomposition of SO_2 gas. Exceeding 2 ppm of SO_2 can have detrimental effects on crops, as it can potentially destroy chloroplasts essential for photosynthesis [11].

To minimize the impact on the environment, it has become a primary goal to reduce anthropogenic SO_x, particularly by desulfurization of flue gas during combustion, as well as to monitor SO_x concentrations in situ at the sources and in the ambient atmosphere. Moreover, air quality monitoring of SO_2 is critical for safety in closed spaces and for leak identification.

Hence, an effective monitoring system is crucial to maintaining SO_2 levels within safe thresholds. To analyze and quantify SO_2 and other sulfur compounds, the conventionally used laboratory technique is gas chromatography coupled with mass spectrometry (GC-MS). GC-MS is acknowledged for its precision and reliability in identifying gaseous compounds, establishing itself as the industry standard. Despite its accuracy, GC-MS presents practical challenges such as the need for bulky and expensive equipment, specialized personnel, and complex pre-treatment processes, resulting in being unsuitable for continuous real-time detections. This underscores the impracticality of such techniques for widespread use in on-site gas monitoring. Therefore, there is a clear need for alternative methods that offer cost-effectiveness, swift processing, rapid response, and reduced reliance on solvents and samples for routine detections.

To date, gas sensors have emerged as both a cost-effective alternative and a complementary system to laboratory-based analyses, providing a rapid and promising solution for SO_2 detection. Notably, electronic nose (e-nose) systems have gained attention for odor assessments, leveraging their versatility and resemblance to the human olfactory system. The implementation of e-noses involves training procedures, with qualified samples to build a database of reference, as well as sensor array optimization, which requires the selection of appropriate devices among the different classes of gas sensors. Recent developments involved the use of electrochemical and non-dispersive infrared (NDIR) sensors for SO_2 detection. However, some limitations by NDIR devices, e.g., short device lifetime, low selectivity, and spectral interference, have prevented their widespread usage.

Metal-oxide semiconductor (MOX)-based chemoresistive gas sensors are a compelling alternative, showcasing not only high sensitivity but also cost-effectiveness, scalable manufacturing, durability, and seamless integration into Internet of Things (IoT) systems [12]. Previous experimental and theoretical works proved that MOX-based nanostructured materials, such as SnO_2, WO_3, and ZnO are potential candidates to detect SO_2 [7,13–18]. Nonetheless, the investigation of MOX for SO_2 detection has been hampered by evidence of irreversible interactions between this analyte and the active groups over the sensing layers [19], resulting in sensor instability and a short lifetime. For instance, Berger et al. [20] demonstrated irreversible sulfate formation on the surface of SnO_2, which was identified as the cause of the irreversibility of the device response after initial SO_2 detection.

Hence, to enhance their sensitivity and selectivity, various approaches, including the doping and/or decoration effect and heterojunction formation, have been investigated for tuning the material properties. In these perspectives, SnO_2-based sensors, containing small amounts of metals such as Ni and Cu, have already been characterized and tested to achieve selective and sensitive detection of SO_2 gas [21,22].

Consequently, to further investigate the potentialities of chemoresistive gas sensors in monitoring SO_2, this study assesses the sensing capability of seven distinct MOX materials. Three of these are pure MOXs, namely, SnO_2, WO_3 and ZnO, to identify the most promising

among them within our measurement system. The best candidate, in terms of sensitivity and selectivity, has been functionalized with noble metals, such as Au, Pt, Pd, and Ag.

2. Materials and Methods

2.1. Chemoresistive Gas Sensors

ZnO, SnO_2, WO_3, SnO_2:Au, SnO_2:Pt, SnO_2:Pd, and SnO_2:Ag were synthesized in powder form by the sol-gel method [23–25]. The powders were mixed with organic excipients, namely, α-terpineol, ethyl cellulose, and silica, to form homogeneous pastes that facilitate the screen-printing technique. The resulting pastes were sonicated for 2 h and then screen-printed onto alumina substrates (defined area of 2.54 × 2.54 mm^2) [26,27]. The semiconducting MOX thick films (around 20–30 µm of thickness) were sintered in air for 2 h at 650 °C to remove the organic precursors and improve mechanical stability and film adhesion. The substrates were equipped with interdigitated gold contacts on the front side, to provide the bias voltage for measuring the conductance of the film, and a platinum heater was integrated on the back side to thermally activate the sensing material at its optimal working temperature. Finally, these substrates were bonded to a standard TO-39 support through thermo-compression of 60 µm of diameter gold wires (Figure S1, Supporting Information). The integration of electrodes and heaters in the alumina substrate allows for precise control and measurement of the sensing material's response.

2.2. Lab-Test Setup

The MOX-based sensors were electrically characterized in a sealed test chamber of volume ≈ 622 cm^3 in which temperature and relative humidity (RH%) were measured by a commercially available Honeywell (Charlotte, NC, USA) HIH-4000 sensor (accuracy ± 3.5 RH%). Firstly, the devices were exposed to synthetic dry air (20% O_2 and 80% N_2) for almost one day in order to obtain the baseline stabilization. Secondly, the mixture of gases from certified cylinders were injected inside the chamber through mass-flow controllers, achieving a total flow of 500 standard cubic centimeters per minute (sccm). The filling time of the test chamber was about 1 min and 15 s, as it depends on the size, the geometry of the chamber, and the velocity of the gas flow. The humidity conditions were obtained by fluxing a fraction of the total synthetic air into a gas bubbler filled with deionized water. Power suppliers from Aim TTi (Glebe Rd, Huntingdon, Cambridgeshire, UK) were used to furnish the requisite electric current to the sensor heater, while a multimeter, the K2000 from Keithley (Cleveland, OH, USA), was utilized to measure the electrical conductance of the sensing film. A constant bias of 5 V was maintained between the two interdigitated gold electrodes. The circuitry employed for data acquisition was structured around an operational amplifier (OA), which serves as a pivotal component in processing the signals. Thanks to the configuration in which the input voltage (V_{in}) and output voltage (V_{out}) values corresponded to the ends of the sensor resistor (R_s) and the applied load resistor (R_f), respectively, the gain was determined by the relationship $\frac{V_{out}}{V_{in}} = -\frac{R_f}{R_S}$. This fundamental expression elucidates the relationship between the V_{in} and V_{out}, facilitating accurate interpretation of the sensor's response. According to A. Rossi et al. [26], the expression for the sensor conductance G_S is given as follows:

$$G_S = \frac{1}{R_S} = -\frac{V_{out}}{R_f \cdot V_{in}} \quad (1)$$

2.3. Sensing Measurements

The sensors performances were proven by making a comprehensive electrical characterization.

First, the best operating temperature of each MOX film was investigated considering their response to 1 ppm of SO_2 at increased working temperatures, ranging from 200 to 450 °C.

Then, in order to study the sensitivity, the films were exposed to several concentrations of SO_2 ranging from 0.5 to 10 ppm under dry conditions. Specifically, to verify possible surface poisoning effects, once achieved the plateau of the signal after the gas injection, the sensors were again exposed to a fully dry air flux to assess the complete recovery of the baseline The sensor response was defined as the following equations for reducing and oxidizing gases, respectively:

$$R = \frac{G_{gas} - G_{air}}{G_{air}} \text{ forreducinggas} \quad (2)$$

$$R = \frac{G_{air} - G_{gas}}{G_{gas}} \text{ foroxidizinggas} \quad (3)$$

where G_{gas} and G_{air} are the conductance values in gas and in air, respectively. The error on the response value was calculated applying error propagation, considering the load resistance tolerance and the instrument uncertainty on the output voltage acquisition. The result was an error of 5% [28].

Due to instrumental limitations, the sensors' response at the TLV-STEL concentration, 0.25 ppm, was not experimentally evaluated. Otherwise, the theoretical Limit of the Detection (LOD) of the best device was determined as 3(RMS noise/R_{air}), where *RMS* noise is the root mean square deviation and R_{air} is the resistance in dry air [29].

Humidity is a very common interference due to its ability to interact with the film, affecting its conductance and generating competitive −OH groups that limit the adsorption sites on the reactive surface. To explore its effect on the sensor performance, 5 ppm of SO_2 was injected into the gas chamber in presence of different percentages of humidity (2–56 RH%).

The stability and repeatability of the best SO_2 devices at its operating temperature was assessed under 6 ppm of the target gas in dry and wet (30 RH%) conditions. The response (τ_{res}) and the recovery (τ_{rec}) times of the sensors were calculated as the times needed to attain 90% of the steady-state response and required to switch back to 90% of the baseline value, respectively.

To verify the influence of possible interfering compounds, they were also exposed to different volatile analytes, such as benzene, ethanol, nitrogen dioxide (NO_2), dimethyl disulfide (DMDS), carbon monoxide (CO), and carbon dioxide (CO_2). The gases and their concentrations were chosen in order to test the surface reactivity of the semiconductors vs. different chemical functional groups. In particular, the concentrations of the potential inteferents were chosen based on TLV-TWA and the American Conference of Governmental Industrial Hygienists (ACGIH) TLV values [30–35].

Moreover, to evaluate the ability of the sensors to detect SO_2 in presence of different analytes, we also performed cross-selectivity measurements. Therefore, the sensors were exposed to 5 ppm of SO_2 in an atmosphere of 1 ppm of ethanol in dry and wet (30 RH%) conditions.

3. Results

3.1. Operational Temperature

The sensors' optimal working temperature was determined by measuring conductance variations before and after introducing 1 ppm of SO_2 in dry conditions across a range of working temperatures from 200–450 °C (Figure 1). The response of ZnO, SnO_2:Pd, SnO_2:Au, SnO_2, SnO_2:Pt, and SnO_2:Ag sensors increased with the temperature rise, reaching the highest value at 400 °C. High operating temperatures are commonly used to lower response and recovery times and to optimize the MOX-based sensors catalytic activity towards SO_2, facilitating surface redox reactions. Nevertheless, beyond the optimal temperature, gas desorption rates rise significantly, leading to further lower sensor response [24].

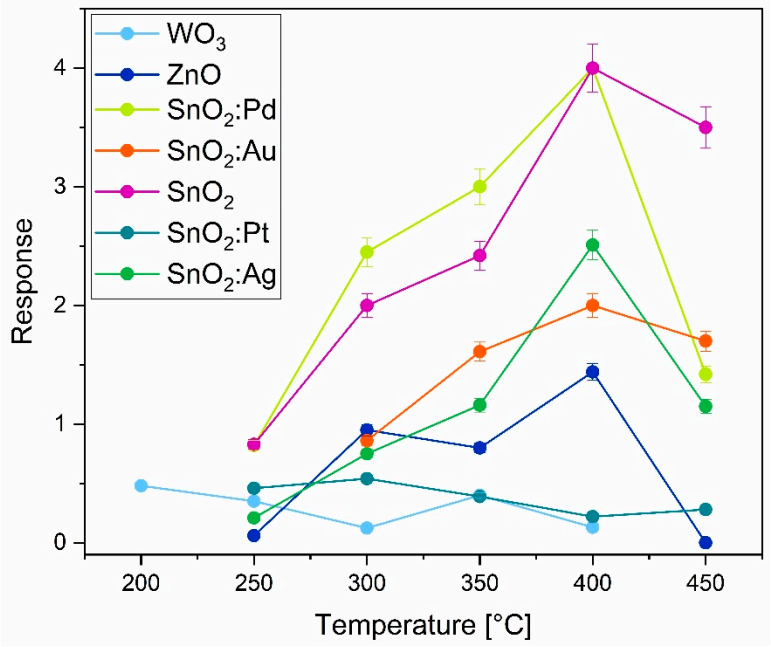

Figure 1. Response vs. working temperature of the sensors to 1 ppm of SO_2 in dry conditions. The temperature and RH% of the chamber are 25–30 °C and 2 RH%, respectively, during the measurements. The response was calculated by Equation (2).

In contrast to the other sensors, WO_3 exhibited two peak responses at 200 °C and 350 °C, suggesting distinct optimal conditions for detecting the analyte, likely due to different active sites on the surface for SO_2 chemisorption, namely, O_2^- at 200 °C and O^- at 350 °C, as explained in our previous work [26] and also deepened in the Discussion section of the present study. However, since the response value at 200 °C and 350 °C is almost the same, the lowest working temperature (200 °C) was selected due to alignment with requirements for low-power consumption in portable and IoT applications.

The optimal temperature for each sensor is summarized in Table 1 and was selected for subsequent comprehensive electrical characterization.

Table 1. Optimal operating temperature of the sensors for SO_2 detection, obtained from Figure 1.

Sensor	Optimal Working Temperature [°C]
WO_3	200
ZnO	400
SnO_2:Pd	400
SnO_2:Au	400
SnO_2	400
SnO_2:Pt	300
SnO_2:Ag	400

Notably, Figure 1 also shows that the SnO_2-based sensor had greater response values than the other pure MOXs, namely, ZnO and WO_3. That had been the underlying motivation for decorating SnO_2 with noble metals rather than ZnO or WO_3.

3.2. Sensitivity

To investigate the sensitivity, we exposed the sensors towards several concentrations of the analyte, in particular, SnO_2:Au, SnO_2:Pd and ZnO from 0.5 to 10 ppm, instead of

SnO_2, SnO_2:Pt and SnO_2:Ag from 1 to 10 ppm. Only WO_3 was tested from 0.5 to 7 ppm since the response tended to remain constant and low. Figure 2 highlights that SnO_2:Au, SnO_2:Pd and SnO_2 sensors at each tested concentration exhibited higher responses than the others and they did not saturate at the relative highest concentration tested. On the other hand, WO_3, ZnO, SnO_2:Ag, and SnO_2:Pt sensors showed a constant response for concentrations above 2 ppm, which can be attributed to the saturation of active sites on the materials and sulfur poisoning of the surface [36]. Therefore, SnO_2:Au, SnO_2:Pd and SnO_2 sensors exhibited a remarkable capability to detect SO_2 across a wide range of concentrations, which make them appropriate for diverse industrial, environmental, and safety monitoring applications.

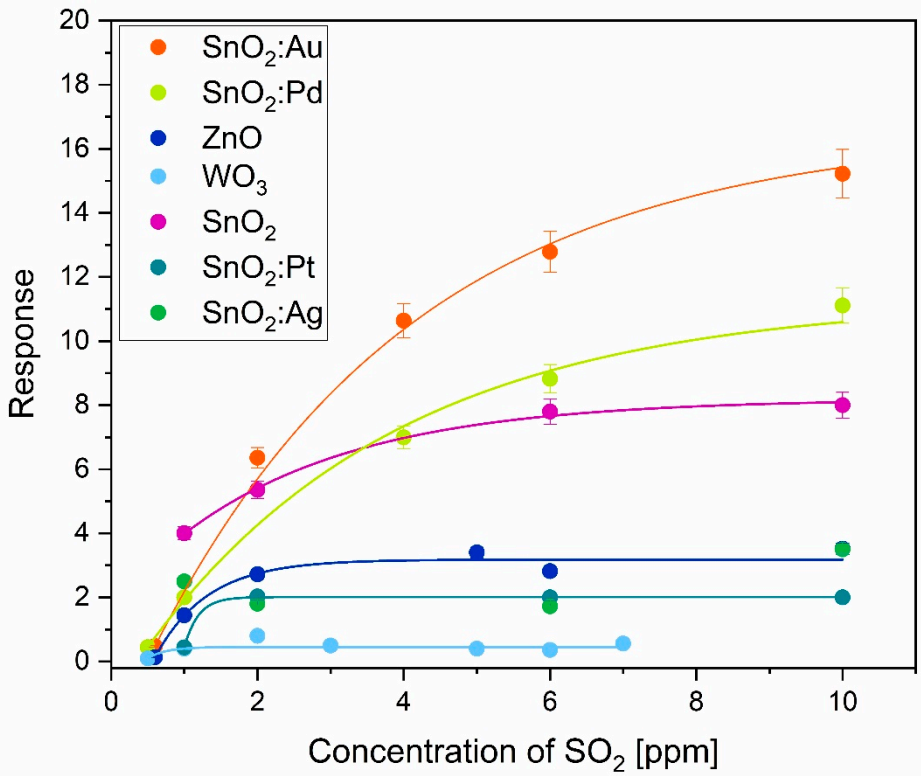

Figure 2. Response vs. several concentrations of SO_2 in dry conditions. The calibration curves of SnO_2:Au, SnO_2:Pd, WO_3, SnO_2, SnO_2:Pt, and ZnO are fitted with asymptotic function.

The calibration curves of the sensors were fitted with asymptotic function ($y = a - b \cdot c^x$), except for the SnO_2:Ag device, for which it was not possible to identify a suitable curve fit. All the metrics parameters of the function are listed in Table S1 (Supporting Information).

In particular, it turned out that the SnO_2:Au sensor showed better responses than the other devices for SO_2 detection with a theoretical LOD of $\sim$ 0.48 ppm. In Figure S2 (Supporting Information), we reported the SnO_2:Au sensor response at three SO_2 concentrations close to its LOD. One can observe that below the LOD, the sensor signal (at 0.2 and 0.3 ppm) was noisy and not stable.

3.3. Humidity Effect

The impact of humidity on the sensing performance was assessed by fluxing 5 ppm of SO_2 while exposing the devices to escalating levels of water vapor (2–56 RH%). As depicted in Figure 3, the responses exhibited a significant drop at 17 RH% due to the competitive reaction for active sites between water molecules and SO_2 [27]. However, for SnO_2-based sensors and ZnO, the response to SO_2 was clearly discernible, with SnO_2:Au exhibiting the strongest signal. Only the WO_3 was not able to detect SO_2 in humid conditions for

values higher than 17 RH%. Starting from 45 RH%, all sensors maintained an almost constant response. This behavior is explainable with the Grotthuss mechanism, in which the formation of continuous water layers over the sensing film hinders the reaction between the analytes and the functional material active sites [37].

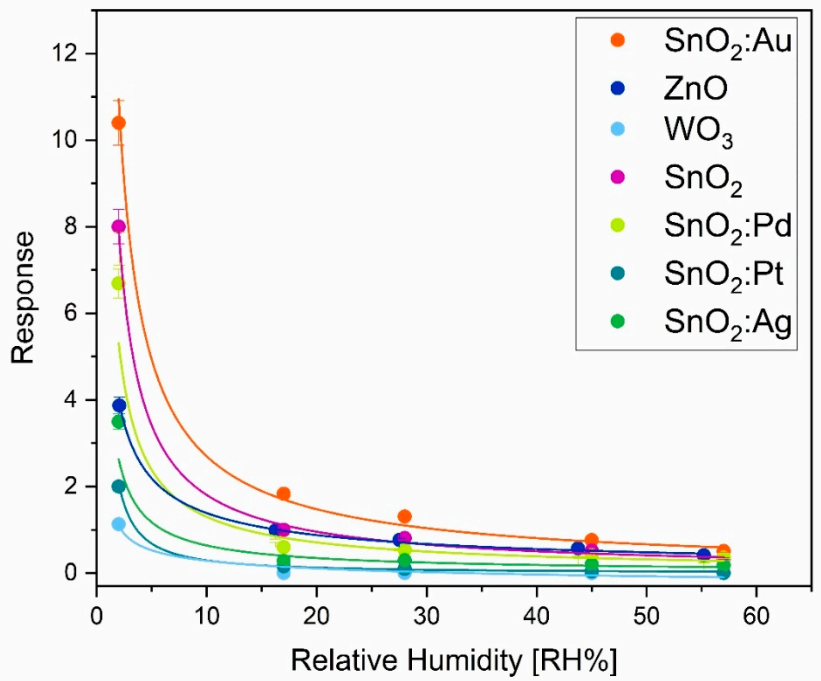

Figure 3. Humidity effect on sensor responses towards 5 ppm of SO_2.

To the best of our knowledge, the only work that deeply discussed the humidity effect in SO_2 detection was developed by Gaiardo et al., who proposed a novel approach using nanostructured silicon carbide (SiC) as a sensing film [28]. It resulted in a highly selective SO_2 sensor even if it operated at a high temperature (600 °C). In this work, they tested five different relative humidities vs. 10 ppm of SO_2. Starting from 2 to 60 RH%, the response remained rather stable around 0.25, reaching a peak of 0.27 at 13 RH%. Moreover, in a consecutive study, M. Della Ciana et al. supported the previous work by Gaiardo et al. applying operando Diffuse Reflectance Infrared Fourier Transform (DRIFT) spectroscopy. With this advanced technique, they demonstrated that the enhancement of SO_2 response under wet conditions was attributed to the formation of SO_x species, which increased the number of charge carriers. However, despite these advancements, especially in SO_2-sensing mechanisms in wet conditions, SiC sensors still exhibited a low response (0.20 at 8 RH%) even to higher concentrations of SO_2, such as 25 ppm [37]. On the contrary, the response at 8 RH% of SnO_2:Au sensor to a SO_2 concentration five times less (5 ppm) is equal to 3.7.

3.4. Repeatability

The stability of the dynamic response vs. 6 ppm of SO_2 during four consecutive cycles was investigated in dry and wet conditions for the best candidate, SnO_2:Au (Figure 4). The film exhibited a clear reversible interaction and good repeatability for detection over time. A doubling increase in the conductance baseline of the sensitive film was observed when exposed to a humid atmosphere due to water's homolytic dissociation. This chemical process involved water interacting with metal sites and lattice oxygen, leading to the formation of terminal and anchored hydroxyl groups (−OH) on the film's surface. These −OH groups acted as surface donors, releasing electrons into the conduction band. This alteration in the surface chemistry affected the film's catalytic properties regarding SO_2 detection by replacing the oxygen ion active sites, typically present in dry conditions, with the newly formed hydroxyl groups.

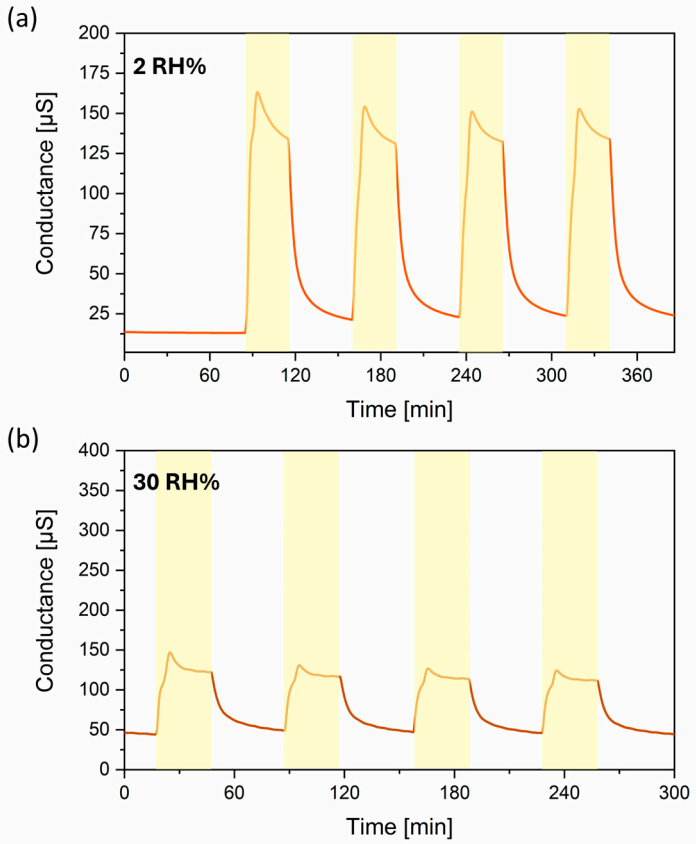

Figure 4. A total of 6 ppm for four SO_2 cycles of SnO_2:Au at (**a**) dry and (**b**) 30% relative humidity.

However, the variation of the conductance values over the four test cycles under SO_2 exposure was similar in dry and wet conditions. Instead, the values of the conductance baseline mainly increased during the test in dry air, while they recovered almost the initial levels during the measurement in humid air. This confirmed that SnO_2:Au sensor can be reliable in real-like conditions limiting the effect of humidity on the signal drift.

The response and recovery times of SnO_2:Au sensors are 3 and 17 min, respectively, in dry conditions, whereas in wet conditions, the response and recovery times are 5 min and 19 min, respectively. These values are in line with those exhibited by common MOX-based gas sensors [24,26].

In addition, Figure 4 shows a similar response shape of the sensor in dry and humid conditions, i.e., a rapid increase when the target gas was introduced. This sharp peak can be ascribed to the dynamic equilibrium between gas diffusion into deeper layers of the sensing material and the kinetic processes of gas adsorption/desorption at its surface [38]. At the initial stage, SO_2 diffuses along the sensing film, starting to influence the dynamic equilibrium of redox reactions occurring at the surface of SnO_2:Au, decreasing, for example, the number of ionized oxygens, resulting in an increase in conductance. Nevertheless, at equilibrium, several factors may influence the conductance in presence of SO_2, slightly lowering its initial value. For instance, the competitive diffusion of new analyte and non-reactive reaction products inside and outside the sensing film should be considered, as well as the kinetic regeneration of active sites.

In order to investigate the long-term stability of the SnO_2:Au sensor, we verify its response value by comparing three different measurements with 3 ppm of SO_2 over a period of 5 months (Figure S3, Supporting Information).

A deepened investigation on SO_2 chemoresistive gas sensors was conducted in order to compare the performance of SnO_2:Au studied in this work with devices already discussed in the literature; see Table 2. Even if it operates at a high temperature, the SnO_2:Au sensor can be obtained with an easier and cheaper synthesis process, such as sol-gel synthesis,

enabling a potential large-scale production than the semiconducting composites explored by other authors mentioned. Moreover, the complete inorganic nature of our sensing material guarantees a strong stability with respect to the organic-based semiconductors. The SnO_2:Au sensor can detect SO_2 over a wide range of concentrations (0.5–10 ppm) and, according to the PEL-TWA (5 ppm), it showed a response at least three times higher than the other devices. Under wet conditions, among the sensing material listed in Table 2, only the Ni/SnO_2 sensor exhibited a comparable response to SnO_2:Au ones, even if the latter demonstrated a negligible influence by humidity over 30 RH%, which makes it suitable for real applications.

Table 2. Comparison of gas detection features exhibited by SO_2 chemoresistive sensors identified in the literature.

Sensing Materials	Operating Temperature [°C]	Concentration [ppm]	Response Formula	Response in Dry/Wet Air	LOD	Reference
rGO/TAPP	RT	5	$(R_{gas} - R_{air})/R_{air}$	-/0.45 at 30 RH%	5 ppm	[39]
Ni/SnO_2	RT	5	R_{gas}/R_{air}	-/2.4 at ~55–65 RH%	-	[19]
rGO	RT	5	$(R_{air} - R_{gas})/R_{air}$	3.21/-	-	[40]
ITO(In_2O_3/SnO_2)	240	5	R_{air}/R_{gas}	-/1.8 at 35 RH%	-	[41]
Ag NWs@SnO_2/CuO	80	50	R_{air}/R_{gas}	2.1/-	0.25 ppm	[42]
GO/ZnO NR	RT	25	R_{gas}/R_{air}	2.97/-	-	[43]
RGO/SnO_2 nanocomposites	60	10	$(R_{air}/R_g) - 1$	1.2/-	-	[44]
SnO_2/NiO	180	500	$(R_{air}/R_g) - 1$	56/50 at dry/70 RH%	-	[45]
Ru/Al_2O_3/ZnO	350	100	$(R_{air} - R_{gas})/R_{air}$	65/-	5 ppm	[46]
NiO:SnO_2	240	100	R_{air}/R_{gas}	10/9.1 at dry/70 RH%	-	[47]
SnO_2:Au	**400**	**5**	$\mathbf{(G_{gas} - G_{air})/G_{air}}$	**10.4/2 at dry/30 RH%**	**0.48 ppm ***	**This work**

The "-" stands for not mentioned in the respective article. R_{air} and R_{gas} are the resistance in dry air and in presence of SO_2, respectively. * Theoretical value.

The SnO_2:Au sensor showed outstanding sensitivity even at a very low concentration. Indeed, the theoretical limit of detection calculated is equal to 0.48 ppm, a value remarkably comparable to that obtained in the Ag NWs@SnO_2/CuO sensor, which reported a LOD of 0.25 ppm.

Concerning the response and recovery times, it was not possible to compare the performance since these values are strongly correlated with geometry and arrangement of the experimental setup, e.g., test chamber volume and gas flow rate.

Therefore, the analysis carried out in this work revealed superior performance of the Au-decorated SnO_2 for the sulfur dioxide detection with respect to the current MOX-based sensors investigated from the literature.

3.5. Selectivity

Moreover, in the practical implementation, one should consider the co-presence of other gases whose physicochemical properties may affect the sensor performance. Therefore, the selectivity of the devices was investigated by exposing the sensors to various interferents, such as benzene (0.5 ppm), ethanol (5 ppm), NO_2 (3 ppm), DMDS (0.25 ppm), CO_2 (5000 ppm) and CO (25 ppm) under dry air. The dynamic signal of output voltage of the sensors for all the measurements are shown in Figures S4–S10

(Supporting Information), together with the load resistances in Table S2. The bar graph in Figure 5 illustrates the response values determined by Equations (2) and (3), to better evaluate the sensor's selectivity.

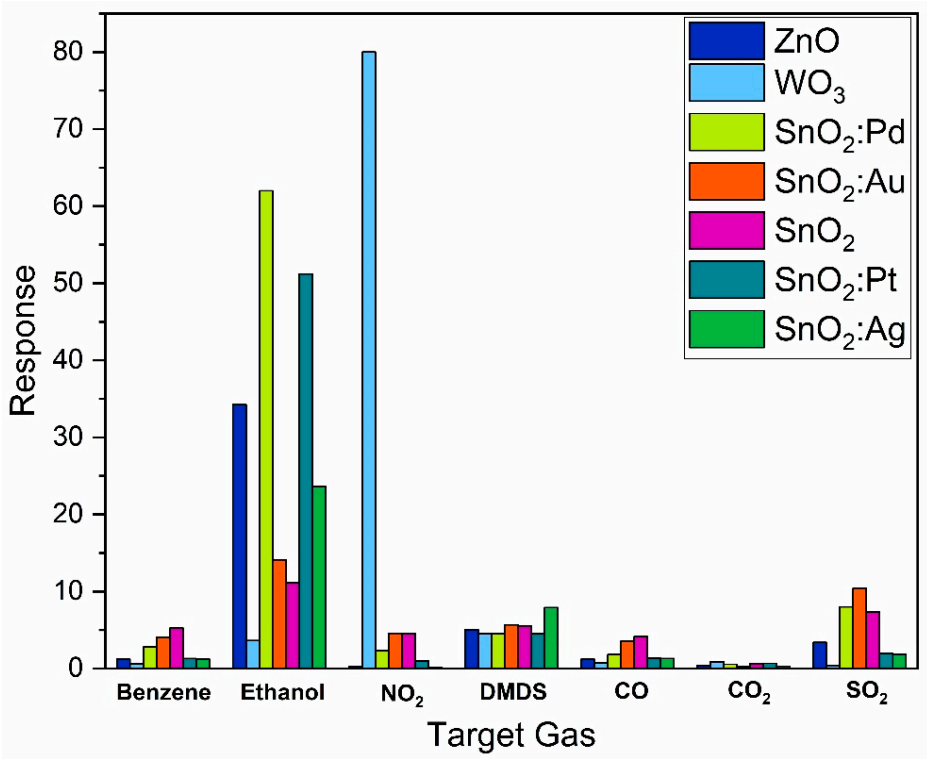

Figure 5. Response of the sensors vs. 0.5 ppm of benzene, 5 ppm of ethanol, 3 ppm of NO_2, 0.25 ppm of DMDS, 25 ppm of CO, 5000 ppm of CO_2, and 5 ppm of SO_2 under dry air condition (≈2 RH%).

As expected, almost all sensors exhibited a high response to ethanol [26,48–50], in particular, SnO_2:Pd, which therefore cannot be defined as selective for SO_2 detection. Among the decorated sensor-based on SnO_2, the SnO_2:Au is the one that exhibited the lowest response value to ethanol. In contrast, all the sensors exhibited negligible responses to CO, CO_2 and benzene. Only SnO_2-based sensors showed superior response to sulfur-containing gases such as DMDS and SO_2, especially SnO_2:Au, which proved to be particularly selective vs. SO_2. Then, WO_3 and ZnO, two of the most common pristine nanostructured MOX materials, were considered unsuitable for SO_2 detection due to their low sensitivity (Figure 2) and stronger selectivity for interfering gases such as ethanol and NO_2 than for the analyte of interest (Figure 5).

3.6. Cross-Selectivity

The cross-selectivity of the sensors towards 5 ppm of SO_2 in the presence of 1 ppm (baseline) of ethanol was performed in dry and wet conditions (30 RH%), as shown in Figure 6. The presence of ethanol as an interferent during the exposure to SO_2 had a notable impact on the response of SnO_2:Au sensors. Comparing Figure 6 to Figure 2, one can observe that the response to 5 ppm of SO_2 decreased from 10.4 to ~2.5 in dry conditions and ~0.5 in wet conditions. This effect can be attributed to competitive reactions between the reactive gases. Indeed, both ethanol and H_2O can react with the material active sites, making them ineffective for detecting SO_2. Furthermore, the products of such reactions, for example chemisorbed alkyl chains, might accumulate over the surface, hysterically hindering nearby active sites. However, SnO_2:Au demonstrated the effective ability to discriminate against SO_2 among ethanol interfering gas.

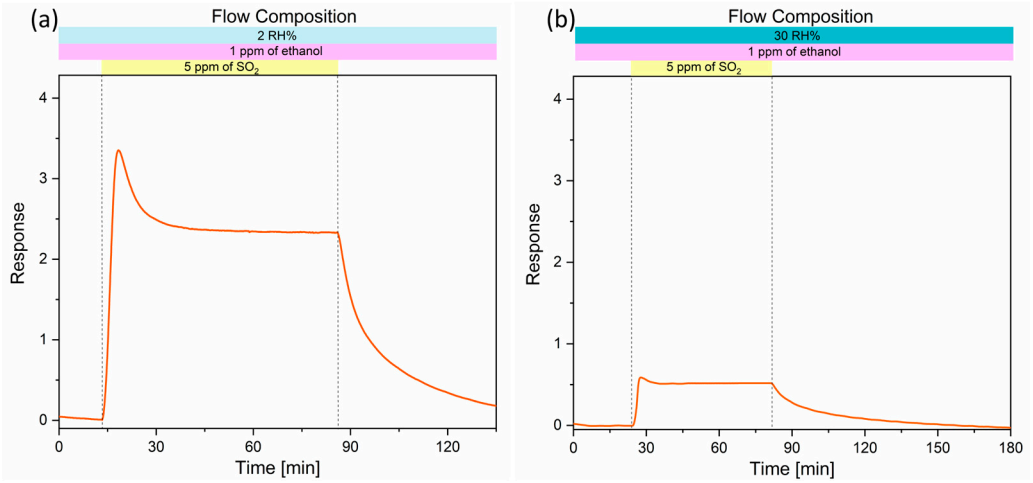

Figure 6. Dynamic sensor responses of SnO_2:Au towards 5 ppm of SO_2 in an atmosphere of 1 ppm of ethanol in (**a**) dry and (**b**) wet conditions (30 RH%). The duration of the measurements depends on the time required for most of the sensors to achieve the steady state in presence of SO_2.

4. Discussion

Gas-sensing mechanisms of metal oxides, such as SnO_2, ZnO, and WO_3 presented in this study, involve complex surface reactions, which are influenced by various intrinsic and extrinsic factors. The intrinsic ones are inherent factors such as (i) activation of chemisorbed active sites from oxidative and reductive reactions, (ii) the creation of acidic or basic centers, and (iii) hydrate–hydroxyl layers, that, synergically combined, play a crucial role [51]. Indeed, (iv) the formation of extrinsic active centers on the surface are due to the modifications by catalytic clusters of noble metals, e.g., Au, Pd, Pt, and Ag.

4.1. Intrinsic Properties

4.1.1. Oxygen Chemisorption

The most common sensing mechanism explaining the response of MOX-based sensors to reducing gases involves oxygen chemisorption and subsequent redox reactions of the analytes with the oxygen-based surface ions. In principle, the oxygen molecules, which are chemisorbed on the semiconductors, ionize into O_2^-, O^-, and O^{2-} anion species by accepting the electrons from MOX materials at different temperatures and decreasing the overall conductance of the sensing film. The oxygen adsorption has been investigated by several works in literature [52], as it follows:

$$(O_2)_{gas} \leftrightarrow (O_2)_{adsorbed} \quad (4)$$

$$(O_2)_{adsorbed} + e^- \leftrightarrow O_2^- \quad (5)$$

$$O_2^- + e^- \leftrightarrow 2O^- \quad (6)$$

$$O^- + e^- \leftrightarrow O^{2-} \quad (7)$$

Oxygen anions O_2^-, O^-, and O^{2-} are stable below 100 °C, 100–300 °C, and above 300 °C, respectively [52]. Based on this consideration, since in the current work, the operating temperature for most of the sensors was 400 °C, it is likely that they exhibited the formation of O^{2-} ions (Figure 7a), except for WO_3, which operates at a low temperature of 200 °C, where the formation of chemisorbed O_2^- and O^- ions was more probable. Differently from the other sensors, WO_3 displayed two maxima responses at 200 °C and 350 °C, meaning that there are two distinct conditions for optimal detection of SO_2, probably characterized by different active sites, namely, O_2^- and O^- ions in the first case and O^- and O^{2-} in the second case. In the temperature range between these two optimal values (200 °C and 350 °C), an unfavorable competition between different reaction mecha-

nisms of the analyte absorption and desorption would lead to a decrease in WO_3-sensing capabilities [26].

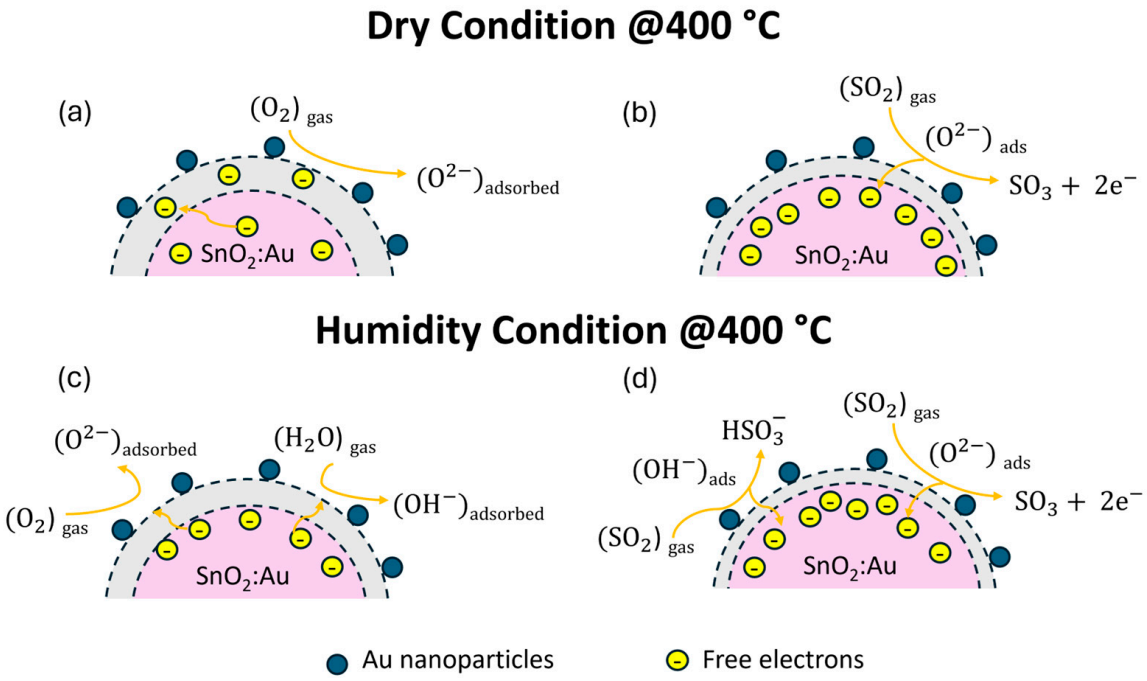

Figure 7. Reaction mechanisms on the surface: (**a**) dry air, (**b**) under SO_2 exposure in dry air, (**c**) wet air, and (**d**) under SO_2 exposure in humid air.

When the sensors were exposed to SO_2 gas molecules in dry conditions, they reacted with the chemisorbed oxygen species on the surface and released the electrons to the conduction band of the MOX material.

In particular, in the case of the sensor that exhibited the best performance in the present work, i.e., SnO_2:Au, the overall surface reaction mechanism was given by the catalytic oxidation of SO_2 to SO_3 at high temperature (400 °C) [28] (see Figure 7b):

$$SO_2 + O^{2-} \leftrightarrow SO_3 + 2e^- \quad (8)$$

From the above reaction, it is clear that when the target gas reacts with the oxygen species adsorbed on the SnO_2:Au surface, the number of free electrons increases, resulting in an increase in conductivity of the material.

4.1.2. Acid and Basic Centers

Beyond the ionosorption and interaction of oxygen species, surface acidity and basicity play a pivotal role in gas-sensing mechanisms. Indeed, functional material active sites can be basic in nature, such as surface oxygen anions and hydroxyl species, or acidic, like coordinately unsaturated cations and −OH Brønsted acid states [53]. The concentration of different active sites influences the adsorption and reaction of target gases on the sensor's surface, thereby affecting its sensitivity and selectivity, as deeply discussed by Marikutsa et al. in [53]. The concentration of Brønsted and Lewis acid sites followed the order $ZnO < SnO_2 < WO_3$, consistent with the increase in metal–oxygen bond energy, electronegativity, and charge/radius ratio of cations. This sequence also reflects the decreasing optical basicity of oxides [53]. The basic nature of ZnO resulted in selectivity for VOCs like ethanol, but poor detection capabilities for sulfur-containing compounds. On the other hand, WO_3, the most acidic in nature, displayed a high response for oxidizing gas, such as NO_2, and very low signals for the other reducing gases. Between the three MOXs, SnO_2 was the most suitable for the development of chemoresistive SO_2 sensors. Berger et al. demonstrated that an increase in surface acidity for SnO_2-based material (probably related to sulfate

formation) after SO_2 exposure may explain the increase in the sensor's sensitivity [20]. Furthermore, enhanced sensitivity of SnO_2-based material was ascribed to the presence of noble metals, such as Au and Pd, which elevate the inherent acidity of pristine SnO_2. Therefore, the intrinsic acid centers of SnO_2, in combination with the extrinsic active centers, i.e., noble metals, effectively affect the sensing performance towards SO_2.

4.1.3. Hydrated Layers

Concerning the gas-sensing mechanism in wet conditions, the presence of H_2O molecules affects the reaction scenario (Figure 7c). Indeed, H_2O molecules (Lewis base) can be adsorbed as are on the surface or interact with cations (Lewis acid) by a strong binding resulting in water molecules dissociation and then producing the −OH groups. In this second case, strong Lewis acidic cations, i.e., W^{6+}, Sn^{4+}, Zn^{2+}, can bind more than one −OH group, then acquire an acidic proton and behave as Brønsted acid site. This leads to an increase in the semiconductors conductance due to the redox reaction, which provides electrons to the sensing materials.

In our case, before the interaction with the sensing films, water molecules can react with SO_2 in the atmosphere by producing H_2SO_3 and further by-products (see Figure 7d). Subsequently, SO_2 and the other gaseous compounds, resulting from the interaction between SO_2 and H_2O, can interact with oxygen and hydroxyl ions adsorbed on the surface of the materials. The competitive reaction between −OH groups and pre-adsorbed oxygen species contribute to reducing the sensitivity of the materials and, as a result, negatively affect the performance of the sensors with respect to the dry ambient.

Furthermore, the consecutive creation of continuous layers of water molecules would hinder the functional material's active sites for reaction with the analyte, thus reducing the sensitivity of the MOX films [37].

4.2. Extrinsic Properties

The presence of noble metals nanoparticles, in particular for SnO_2:Au sensors, exhibited a good catalytic dissociation performance for oxygen, which promoted the formation of chemically adsorbed oxygen on the material surface [54]. Thus, the reaction rate between chemically adsorbed oxygen and SO_2 increased, and the space charge layer narrowed accordingly. This further improved the response of the sensor to SO_2.

A further crucial aspect concerns the fact that the SnO_2:Au, thanks to the low chemical affinity between Au nanoparticles and sulfur atoms, is capable of preventing irreversible poisoning of the sensing film surface due to the formation of strong metal–sulfide bonds [36].

On the other hand, among SnO_2-based gas sensors tested, SnO_2:Ag demonstrated a constant response with increasing SO_2 concentrations, which is probably due to the production of sulfur stable compounds with Ag metals such as Ag_2S consequently poisoning the reactive surface from 2 ppm.

5. Conclusions

The experimentation performed in the present work could guide future developments on modified MOX-based sensors and open new frontiers for olfactory systems dedicated to SO_2 monitoring in a wide range of concentrations and in real-world applications. ZnO and WO_3 were proven to be selective to different gases and therefore not appropriate for SO_2 detection. In contrast, SnO_2 was more suitable for the detection of sulfur-containing gases. Therefore, SnO_2 was decorated with different noble metals. Addition of Ag or Pt seems to poison the surface, leading to worse sensing performances than pure SnO_2. On the other hand, Pd and Au have been demonstrated to be effective in improving the performance of pure SnO_2. In particular, SnO_2:Au highlighted good sensitivity, cross-selectivity, and humidity-independent behavior for concentrations above 17 RH%. The enhanced reactivity could be explained by the decoration of the SnO_2 surface with Au nanoparticles that positively affected the concentration of active sites and acid-base properties of the surface.

The effect of catalytic additives on the intrinsic and extrinsic active centers of SnO_2 is an important factor that determines the proper conditions for an effective gas-solid interaction. In fact, modification with Au has different effects on the concentration and reactivity of the active sites of pristine SnO_2. As a result, modification with Au may cause an increase in the concentration of chemisorbed oxygen species and acid sites, which are the centers of interaction with SO_2. Therefore, for the future works, additional studies should be performed under controlled conditions in the presence of the target molecules with the use of in situ or operando techniques, such as operando DRIFT spectroscopy, or chemisorption analysis to explore the active sites of the material in depth.

Supplementary Materials: The following supporting information can be downloaded at: https://www.mdpi.com/article/10.3390/chemosensors12060111/s1, Figure S1: Schematic representation of sensor fabrication; Table S1: The parameters of the calibration fit shown in Figure 2 for ZnO, WO_3, SnO_2:Pd, SnO_2:Au, SnO_2, and SnO_2:Pt sensors; Table S2: Load resistances of sensors during selectivity measurements; Figure S2: Response to three different concentrations of SO_2 around the theoretical LOD of SnO_2:Au sensor; Figure S3: Response to 3 ppm of SO_2 obtained for SnO_2:Au sensor tested with three different measurements over a period of five months; Figure S4: V_{out} response vs. 0.25 ppm of DMDS; Figure S5: V_{out} response vs. 5 ppm of ethanol. In the case of WO_3, the injection of the gas was different due to a different day of measurement; Figure S6: V_{out} response vs. 5000 ppm of CO_2. In the case of WO_3, the injection of the gas was different due to a different day of measurement; Figure S7: V_{out} response vs. 3 ppm of NO_2. In the case of WO_3, the injection of the gas was different due to a different day of measurement; Figure S8: V_{out} response vs. 0.5 ppm of benzene. In the case of WO_3, the injection of the gas was different due to a different day of measurement; Figure S9: V_{out} response vs. 25 ppm of CO. In the case of WO_3, the injection of the gas was different due to a different day of measurement; Figure S10: V_{out} response vs. 5 ppm of SO_2. In the case of WO_3, the injection of the gas was different due to a different day of measurement.

Author Contributions: Conceptualization, A.R. and B.F.; validation, A.R.; formal analysis, A.R.; investigation, A.R. and A.V.; data curation, A.R.; writing—original draft preparation, A.R. and B.F.; writing—review and editing, E.S. and D.A.; supervision, V.G. and M.M.; funding acquisition, V.G. and B.F. All authors have read and agreed to the published version of the manuscript.

Funding: This research was funded by POR FSE 2014/2020 by Regione Emilia-Romagna, by PNRR ex D.M. 117 02/03/2023, and by University of Ferrara (FIRD 2022).

Institutional Review Board Statement: Not applicable.

Informed Consent Statement: Not applicable.

Data Availability Statement: The original contributions presented in the study are included in the article/Supplementary Material, further inquiries can be directed to the corresponding authors.

Conflicts of Interest: The authors declare no conflicts of interest.

References

1. Mathieu, Y.; Tzanis, L.; Soulard, M.; Patarin, J.; Vierling, M.; Molière, M. Adsorption of SO_x by Oxide Materials: A Review. *Fuel Process. Technol.* **2013**, *114*, 81–100. [CrossRef]
2. Meng, Z. Oxidative Damage of Sulfur Dioxide on Various Organs of Mice: Sulfur Dioxide Is a Systemic Oxidative Damage Agent. *Inhal. Toxicol.* **2003**, *15*, 181–195. [CrossRef] [PubMed]
3. Barnett, A.G.; Williams, G.M.; Schwartz, J.; Neller, A.H.; Best, T.L.; Petroeschevsky, A.L.; Simpson, R.W. Air Pollution and Child Respiratory Health: A Case-Crossover Study in Australia and New Zealand. *Am. J. Respir. Crit. Care Med.* **2005**, *171*, 1272–1278. [CrossRef] [PubMed]
4. Occupational Safety and Health Administration. Available online: https://www.Osha.Gov/Chemicaldata/549 (accessed on 9 May 2024).
5. López-Cervantes, V.B.; López-Olvera, A.; Obeso, J.L.; Torres, I.K.; Martínez-Ahumada, E.; Carmona-Monroy, P.; Sánchez-González, E.; Solís-Ibarra, D.; Lima, E.; Jangodaz, E.; et al. Robust Co(II)-Based Metal–Organic Framework for the Efficient Uptake and Selective Detection of SO_2. *Chem. Mater.* **2024**, *36*, 2735–2742. [CrossRef]
6. Hansell, A.; Oppenheimer, C. Health Hazards from Volcanic Gases: A Systematic Literature Review. *Arch. Environ. Health* **2004**, *59*, 628–639. [CrossRef] [PubMed]

7. Khan, M.; Rao, M.; Li, Q. Recent Advances in Electrochemical Sensors for Detecting Toxic Gases: NO_2, SO_2 and H_2S. *Sensors* **2019**, *19*, 905. [CrossRef] [PubMed]
8. Morulane, K.L.; Swart, H.C.; Motaung, D.E. A Review on Topical Advancement and Challenges of Indium Oxide Based Gas Sensors: Future Outlooks. *J. Environ. Chem. Eng.* **2024**, *12*, 112144. [CrossRef]
9. Dey, S.; Mehta, N.S. Automobile Pollution Control Using Catalysis. *Resour. Environ. Sustain.* **2020**, *2*, 100006. [CrossRef]
10. Lan, W.; Rao, Y.; Zhao, X.; Zhao, Y.; Min, X.; Wu, Y.; Jiang, Z.; Li, T.; Li, Y.; Chen, H.; et al. Rapid Visual Detection of Sulfur Dioxide Residues in Food Using Acid-Sensitive CdTe Quantum Dots-Loaded Alginate Hydrogel Beads. *Food Chem.* **2024**, *446*, 138791. [CrossRef]
11. Peter Singh, L.; Gill, S.S.; Gill, R.; Tuteja, N. Mechanism of Sulfur Dioxide Toxicity and Tolerance in Crop Plants. In *Improving Crop Resistance to Abiotic Stress*; Tuteja, N., Gill, S.S., Tiburcio, A.F., Tuteja, R., Eds.; Wiley: New York, NY, USA, 2012; pp. 133–163. ISBN 978-3-527-32840-6.
12. Pecunia, V.; Petti, L.; Andrews, J.; Ollearo, R.; Gelinck, G.H.; Nasrollahi, B.; Jailani, J.M.; Li, N.; Kim, J.H.; Ng, T.N.; et al. Roadmap on Printable Electronic Materials for Next-Generation Sensors. *Nano Futures* **2024**. [CrossRef]
13. Zhang, H.; Yu, L.; Li, R.; Zhao, F.; Guo, L.; Wang, P.; Cao, W.; Ding, Z.; Qiao, Z. Layer-Tunable Synthesis of Tetragonal Pr-Doped SnO_2 Nanoplates for Enhanced Sensitive SO_2 Sensor. *Sens. Actuators B Chem.* **2024**, *409*, 135629. [CrossRef]
14. Shin, D.; Besmann, T.M.; Armstrong, B.L. Phase Stability of Noble Metal Loaded WO_3 for SO_2 Sensor Applications. *Sens. Actuators B Chem.* **2013**, *176*, 75–80. [CrossRef]
15. Cao, L.; Yu, L.; Li, S.; Nan, N.; Zhang, C.; Fan, X. In-Situ Growth of Well-Ordered ZnO Nanowire-Networks with Interconnected Junctions for Enhanced SO_2 Gas Sensing Properties. *Appl. Surf. Sci.* **2024**, *646*, 158899. [CrossRef]
16. Minh, L.H.; Thuy Thu, P.T.; Thanh, B.Q.; Hanh, N.T.; Thu Hanh, D.T.; Van Toan, N.; Hung, C.M.; Van Duy, N.; Van Tong, P.; Hoa, N.D. Hollow ZnO Nanorices Prepared by a Simple Hydrothermal Method for NO_2 and SO_2 Gas Sensors. *RSC Adv.* **2021**, *11*, 33613–33625. [CrossRef]
17. Franco, M.A.; Conti, P.P.; Andre, R.S.; Correa, D.S. A Review on Chemiresistive ZnO Gas Sensors. *Sens. Actuators Rep.* **2022**, *4*, 100100. [CrossRef]
18. Kanan, S.; Obeideen, K.; Moyet, M.; Abed, H.; Khan, D.; Shabnam, A.; El-Sayed, Y.; Arooj, M.; Mohamed, A.A. Recent Advances on Metal Oxide Based Sensors for Environmental Gas Pollutants Detection. *Crit. Rev. Anal. Chem.* **2024**, 1–34. [CrossRef]
19. Das, S.; Girija, K.G.; Debnath, A.K.; Vatsa, R.K. Enhanced NO_2 and SO_2 Sensor Response under Ambient Conditions by Polyol Synthesized Ni Doped SnO2 Nanoparticles. *J. Alloys Compd.* **2021**, *854*, 157276. [CrossRef]
20. Berger, F.; Fromm, M.; Chambaudet, A.; Planade, R. Tin Dioxide-Based Gas Sensors for SO_2 Detection: A Chemical Interpretation of the Increase in Sensitivity Obtained after a Primary Detection. *Sens. Actuators B Chem.* **1997**, *45*, 175–181. [CrossRef]
21. Zhao, C.; Gong, H.; Niu, G.; Wang, F. Ultrasensitive SO_2 Sensor for Sub-Ppm Detection Using Cu-Doped SnO_2 Nanosheet Arrays Directly Grown on Chip. *Sens. Actuators B Chem.* **2020**, *324*, 128745. [CrossRef]
22. Tyagi, P.; Sharma, A.; Tomar, M.; Gupta, V. Metal Oxide Catalyst Assisted SnO_2 Thin Film Based SO_2 Gas Sensor. *Sens. Actuators B Chem.* **2016**, *224*, 282–289. [CrossRef]
23. Gaiardo, A.; Krik, S.; Valt, M.; Fabbri, B.; Tonezzer, M.; Feng, Z.; Guidi, V.; Bellutti, P. Development of a Sensor Array Based on Pt, Pd, Ag and Au Nanocluster Decorated SnO_2 for Precision Agriculture. *Meet. Abstr.* **2021**, *MA2021-01*, 1550. [CrossRef]
24. Spagnoli, E.; Krik, S.; Fabbri, B.; Valt, M.; Ardit, M.; Gaiardo, A.; Vanzetti, L.; Della Ciana, M.; Cristino, V.; Vola, G.; et al. Development and Characterization of WO_3 Nanoflakes for Selective Ethanol Sensing. *Sens. Actuators B Chem.* **2021**, *347*, 130593. [CrossRef]
25. Gaiardo, A.; Fabbri, B.; Giberti, A.; Guidi, V.; Bellutti, P.; Malagù, C.; Valt, M.; Pepponi, G.; Gherardi, S.; Zonta, G.; et al. ZnO and Au/ZnO Thin Films: Room-Temperature Chemoresistive Properties for Gas Sensing Applications. *Sens. Actuators B Chem.* **2016**, *237*, 1085–1094. [CrossRef]
26. Rossi, A.; Spagnoli, E.; Tralli, F.; Marzocchi, M.; Guidi, V.; Fabbri, B. New Approach for the Detection of Sub-Ppm Limonene: An Investigation through Chemoresistive Metal-Oxide Semiconductors. *Sensors* **2023**, *23*, 6291. [CrossRef]
27. Rossi, A.; Fabbri, B.; Spagnoli, E.; Gaiardo, A.; Valt, M.; Ferroni, M.; Ardit, M.; Krik, S.; Pedrielli, A.; Vanzetti, L.; et al. Functionalization of Indium Oxide for Empowered Detection of CO_2 over an Extra-Wide Range of Concentrations. *ACS Appl. Mater. Interfaces* **2023**, *15*, 33732–33743. [CrossRef]
28. Gaiardo, A.; Fabbri, B.; Giberti, A.; Valt, M.; Gherardi, S.; Guidi, V.; Malagù, C.; Bellutti, P.; Pepponi, G.; Casotti, D.; et al. Tunable Formation of Nanostructured SiC/SiOC Core-Shell for Selective Detection of SO_2. *Sens. Actuators B Chem.* **2020**, *305*, 127485. [CrossRef]
29. Spagnoli, E.; Gaiardo, A.; Fabbri, B.; Valt, M.; Krik, S.; Ardit, M.; Cruciani, G.; Della Ciana, M.; Vanzetti, L.; Vola, G.; et al. Design of a Metal-Oxide Solid Solution for Sub-Ppm H_2 Detection. *ACS Sens.* **2022**, *7*, 573–583. [CrossRef]
30. Occupational Safety and Health Administration. Available online: https://www.Osha.Gov/Chemicaldata/491 (accessed on 9 May 2024).
31. Centers for Disease Control and Prevention, The National Institute for Occupational Safety and Health. Available online: https://www.Cdc.Gov/Niosh/Idlh/10102440.Html (accessed on 9 May 2024).
32. American Conference of Governmental Industrial Hygienist. Available online: https://www.Acgih.Org/Carbon-Monoxide-3/ (accessed on 9 May 2024).

33. American Conference of Governmental Industrial Hygienist. Available online: https://www.Acgih.Org/Carbon-Dioxide/ (accessed on 9 May 2024).
34. Occupational Safety and Health Administration. Available online: https://www.Osha.Gov/Chemicaldata/911 (accessed on 9 May 2024).
35. Centers for Disease Control and Prevention, The National Institute for Occupational Safety and Health. Available online: https://www.Cdc.Gov/Niosh/Pel88/10102-44.Html (accessed on 9 May 2024).
36. Rodriguez, J. The Chemical Properties of Bimetallic Surfaces: Importance of Ensemble and Electronic Effects in the Adsorption of Sulfur and SO_2. *Prog. Surf. Sci.* **2006**, *81*, 141–189. [CrossRef]
37. Ciana, M.D.; Valt, M.; Fabbri, B.; Gaiardo, A.; Spagnoli, E.; Krik, S.; Bernardoni, P.; Gilli, N.; Migliori, A.; Quaranta, A.; et al. SO_2 Sensing Mechanism of Nanostructured SiC-SiOxC Core Shell: An Operando DRIFT Investigation. *Sens. Actuators B Chem.* **2022**, *371*, 132497. [CrossRef]
38. Fu, X.; Liu, J.; Han, T.; Zhang, X.; Meng, F.; Liu, J. A Three-Dimensional Hierarchical CdO Nanostructure: Preparation and Its Improved Gas-Diffusing Performance in Gas Sensor. *Sens. Actuators B Chem.* **2013**, *184*, 260–267. [CrossRef]
39. Khune, A.S.; Padghan, V.; Bongane, R.; Narwade, V.N.; Dole, B.N.; Ingle, N.N.; Tsai, M.-L.; Hianik, T.; Shirsat, M.D. Highly Selective Chemiresistive SO_2 Sensor Based on a Reduced Graphene Oxide/Porphyrin (rGO/TAPP) Composite. *J. Electron. Mater.* **2023**, *52*, 8108–8123. [CrossRef]
40. Kumar, R.; Kaur, A. Chemiresistive Gas Sensors Based on Thermally Reduced Graphene Oxide for Sensing Sulphur Dioxide at Room Temperature. *Diam. Relat. Mater.* **2020**, *109*, 108039. [CrossRef]
41. Peng, K.; Li, Q.; Ma, M.; Li, N.; Sheng, H.; Li, H.; Huang, Y.; Yun, F. Acidic Gas Determination Using Indium Tin Oxide-Based Gas Sensors. *Sensors* **2024**, *24*, 1286. [CrossRef] [PubMed]
42. Yang, J.; Wang, T.; Zhu, C.; Yin, X.; Dong, P.; Wu, X. AgNWs@SnO_2/CuO Nanocomposites for Ultra-Sensitive SO_2 Sensing Based on Surface Acoustic Wave with Frequency-Resistance Dual-Signal Display. *Sens. Actuators B Chem.* **2023**, *375*, 132966. [CrossRef]
43. Dhingra, V.; Kumar, S.; Kumar, R.; Garg, A.; Chowdhuri, A. Room Temperature SO_2 and H_2 Gas Sensing Using Hydrothermally Grown GO–ZnO Nanorod Composite Films. *Mater. Res. Express* **2020**, *7*, 065012. [CrossRef]
44. Tyagi, P.; Sharma, A.; Tomar, M.; Gupta, V. A Comparative Study of RGO-SnO_2 and MWCNT-SnO_2 Nanocomposites Based SO_2 Gas Sensors. *Sens. Actuators B Chem.* **2017**, *248*, 980–986. [CrossRef]
45. Tyagi, P.; Sharma, A.; Tomar, M.; Gupta, V. SnO_2 Thin Film Sensor Having NiO Catalyst for Detection of SO_2 Gas with Improved Response Characteristics. *Sens. Actuators B Chem.* **2017**, *248*, 998–1005. [CrossRef]
46. Liu, Y.; Xu, X.; Chen, Y.; Zhang, Y.; Gao, X.; Xu, P.; Li, X.; Fang, J.; Wen, W. An Integrated Micro-Chip with Ru/Al_2O_3/ZnO as Sensing Material for SO_2 Detection. *Sens. Actuators B Chem.* **2018**, *262*, 26–34. [CrossRef]
47. Fu, Y.; Li, J.; Xu, H. SnO2 Recycled from Tin Slime for Enhanced SO_2 Sensing Properties by NiO Surface Decoration. *Mater. Sci. Semicond. Process.* **2020**, *114*, 105073. [CrossRef]
48. Ivanov, P.; Llobet, E.; Vilanova, X.; Brezmes, J.; Hubalek, J.; Correig, X. Development of High Sensitivity Ethanol Gas Sensors Based on Pt-Doped SnO_2 Surfaces. *Sens. Actuators B Chem.* **2004**, *99*, 201–206. [CrossRef]
49. Dhongade, V.; Sharma, L.; Kahandal, A.; Aiyer, R.C.; Rajdeo, K.; Tagad, C. Pd Doped SnO_2 Based Room Temperature Operable Resistive Sensor for the Detection of Ethanol Vapors. *Mater. Today Proc.* **2021**, *46*, 6437–6444. [CrossRef]
50. Aleksanyan, M.; Sayunts, A.; Shahkhatuni, G.; Simonyan, Z.; Shahnazaryan, G.; Aroutiounian, V. Gas Sensor Based on ZnO Nanostructured Film for the Detection of Ethanol Vapor. *Chemosensors* **2022**, *10*, 245. [CrossRef]
51. Gaskov, A.; Rumyantseva, M.; Marikutsa, A. *Tin Oxide Materials: Synthesis, Properties, and Applications*; Elsevier: Amsterdam, The Netherlands, 2020; Chapter 7; pp. 163–212. [CrossRef]
52. Sahm, T.; Gurlo, A.; Bârsan, N.; Weimar, U. Basics of Oxygen and SnO_2 Interaction; Work Function Change and Conductivity Measurements. *Sens. Actuators B Chem.* **2006**, *118*, 78–83. [CrossRef]
53. Marikutsa, A.; Rumyantseva, M.; Konstantinova, E.A.; Gaskov, A. The Key Role of Active Sites in the Development of Selective Metal Oxide Sensor Materials. *Sensors* **2021**, *21*, 2554. [CrossRef]
54. Wu, Z.; Wang, Y.; Wang, P.; Cheng, X.; Wang, Q.; Yang, Y.; Luo, Y.; An, B.; Xie, E. UV Irradiation of Au-Modified SnO_2 Nanorods Enabling the Rapid Detection of Low-Concentration NO_2 at Room Temperature. *IEEE Sens. J.* **2023**, *23*, 1803–1808. [CrossRef]

Disclaimer/Publisher's Note: The statements, opinions and data contained in all publications are solely those of the individual author(s) and contributor(s) and not of MDPI and/or the editor(s). MDPI and/or the editor(s) disclaim responsibility for any injury to people or property resulting from any ideas, methods, instructions or products referred to in the content.